UK Atomic Energy Authority

ExCALIBUR

Equations for ExCALIBUR/NEPTUNE Proxyapps

Version 1.1

Abstract
The report describes equations for ExCALIBUR project NEPTUNE Proxyapps. The numbering of the systems follows that of the NEPTUNE Science Plan, so that those listed under FM-WP2 are denoted 2-1, 2-2, etc., and under FM-WP3 as 3-1, 3-2, etc. It is a living document to which further equation systems will be added throughout the course of the project.

UKAEA REFERENCE AND APPROVAL SHEET

	Client Reference:	
	UKAEA Reference:	CD/EXCALIBUR-FMS/021
	Issue:	1.01
	Date:	6 May 2021
Project Name: ExCALIBUR Fusion Modelling System		

	Name and Department	Signature	Date
Prepared By:	Wayne Arter BD		6 May 2021
Reviewed By:	Rob Akers Advanced Computing Dept. Manager		6 May 2021
Approved By:	Rob Akers Advanced Computing Dept. Manager		6 May 2021

1 Introduction

Rather than attempting to develop a fully 3-D Exascale targeted plasma edge (or boundary) code from day one, project NEPTUNE will first focus upon the development of "proxyapps" [1], developed by partners across the project through a series of Grant calls. These must be designed and encoded to pave the way to the fully 3-D, actionable and performant NEPTUNE code (or codes) outlined in the Science Plan. As such, all NEPTUNE proxyapps must capture the functionality and performance/scalability characteristics of the eventual infrastructure as much as possible. In addition, all of the solutions across the NEPTUNE programme must eventually be synergistic, leading to an integrated solution for the eventual code(s) – this will require close cooperation through co-design across all partner organisations. The baseline proxyapps for the initial years of the project are described briefly in the Science Plan [2], and expanded upon below to give the "baseline plan" model equations, geometry and boundary conditions. Note, the baseline plan does not preclude additional functionality that any bidder may deem useful (or even essential) to the project. Bidders are encouraged in their response to calls to be creative and ambitious and to describe their own ideas and plans for delivering above and beyond core scope, provided the aim is to increase impact, quality, reduce risk and/or accelerate delivery (and that deliverables are fully aligned with the goals of the NEPTUNE Science Plan [2]).

At baseline, proxyapps target $x86$ (and ideally IBM POWER and ARM CPU) architectures (multi-core and multiple node) for scalability to first generation Exascale hardware. Proxyapps might also target other Exascale candidate architectures (eg. GPGPU) and/or demonstrate a capability to explore the use of novel hardware as it becomes available to the ExCALIBUR project as part of the novel test-bed programme. In order to execute efficiently on parallel architectures, proxyapps are expected to examine use of MPI, OpenMP or some other software technology (ideally with a focus upon performance portability).

Supporting information regarding Braginskii's transport coefficients for plasma in a strong magnetic field appears in Section 2. A description of sources of atomic and molecular radiation is given as an annex in Section A.

1.1 Overall Plan

In the Science Plan [2] the description of work extending beyond Y3 (early 2022) is deliberately vague on the subject of "gyrokinetics", as no widely accepted model for the tokamak edge appears to be available as of early Y2, and even should one appear, it might not be suitable for use in Y3 in NEPTUNE.

As listed, the proxyapps correspond to Plan A, which assumes that no suitable gyroaveraged model will emerge in time, hence *kinetic* implies Particle-in-Cell (PIC). PIC approaches, where charge conservation is vital to control errors, can anyway usefully be pursued for modelling low collisionality plasma species, and should simplify nicely to treat neutral species with long mean-free-paths in tokamak edge problems where mass conservation has been discovered to be critical. Moreover in the context of classical fluid dynamics, the transition from fluid to particles, or short to long mean-free-path, has been well-studied because of the application to the space vehicle re-entry problem and related hypersonic situations. Thus the hybrid fluid/PIC approach might be

regarded as a relatively low-risk route to achieving a robust numerical algorithm.

Evidently full-orbit PIC has the potential to be extremely inefficient relative to gyroaveraged kinetic theory because of the need to follow gyro-orbits in detail. Hence if this can be avoided, either through gyroaveraging or clever numerics or indeed a combination of both, then Plan B will see *kinetic* imply gyroaveraged kinetic theory for modelling plasma species in the proxyapps.

Regarding implementation at the Exascale there is also a conservative Plan A approach which sees the use of relatively simple data structures such as scalar and vector arrays to transfer data, and consequent use of existing code-coupling technologies. Plan B is an aggressive approach to implementation which sees custom data structures allowing for all physical data (particle arrays and fluid field vectors) colocated near a point to be held close in memory, permitting very tight custom code-coupling. As with the *kinetic* options, this Plan B promises significantly faster solutions than the corresponding Plan A, but its adoption depends on the outcome of research work to de-risk.

1.2 Proxyapps Summary

The overall thinking behind the proxyapps is to explore potential 'roadblocks' to the Exascale as early and in as simple a context as is possible, beginning with algorithmic roadblocks. NEPTUNE is directed towards producing 'actionable' code as the basis for large procurements, whereas more physics-focussed software projects conducted by the worldwide nuclear fusion have already advanced to greater complexity, minimising the risk that unexpected problems will appear in the full model.

The numbering of proxyapps below corresponds to the Science Plan.

2-1 2-D model of anisotropic heat transport. It is important to determine early the degree of anisotropy that high-order elements can treat without special coding. If this is unsatisfactorily small, then there are implications for geometry input as well as algorithmic developments that are best addressed as early as possible.

2-2 2-D elliptic solver in complex geometry. One of the indicated elliptic solvers is Grad-Shafranov to produce high order ('spectrally') accurate magnetic fields for use in many other proxyapps. Since Sovinec [3] has already produced a spectral element Grad-Shafranov code, the corresponding NEPTUNE development should mainly serve to identify practical issues concerning implementing high order fe models. The second solver additionally presents a chance to explore comparatively novel meshing techniques developed under Activity A2.1, and later the preconditioning techniques of A2.7.

2-3 1-D fluid solver with simplified physics but with UQ and realistic boundary conditions. This will determine the capability of spectral/hp element to handle sonic outflow boundary conditions needed to represent sheaths, together with large source terms, as well as identifying practical issues concerning intrusive UQ. This software is already potentially useful in its own right for example in modelling MAST-U divertor, and other workers might be drawn in to add additional physical effects to this end.

2-4 Spatially 1-D plasma model incorporating velocity space effects. From the numerical analytic point-of-view, this is a key demonstration of spectral/hp element capability to handle particle interactions. However, again this could be a basis for divertor modelling, to explore sheath effects depending on fieldline incidence on surface, and with minor modification the spread of particle energy around tile edges and corners as performed by Gunn et al [4, 5] for ITER application.

2-5 Spatially 1-D multispecies plasma model. Multispecies throws up a surprising number of issues concerning data definitions (eg. changes to the Coulomb logarithm), structures to deal with different number of species, and perhaps most significantly, complicated inter-species interaction terms both within and at the domain boundaries. This is also an opportunity to mix fluid and *kinetic* representations of *different* species within the *volume*.

2-6 Spatially 2-D plasma model incorporating velocity space effects. With the 1-D multispecies fluid work's having made the generalisation to 2-D straightforward, the challenge here is to start writing a complex proxyapp in production mode, incorporating the research put into design, documentation, code generation and benchmarking. There is an opportunity to study species with both fluid and *kinetic* representations depending on location relative to the wall. Again this is potentially a useful tool in its own right, capable of revealing deficiencies in previous 2-D modelling work.

2-7 Interaction between models of different dimensionality. This should verify that the design has the right data structures to handle additional further complexity beyond intrusive and ensemble-based UQ and model order reduction. The hopefully burgeoning NEPTUNE community could develop this into a design tool with a capability both to explore a large area of tokamak edge parameter space quickly in 0-D or 1-D and also to focus on relatively small but critical 2-D features, such as tile edges.

2-8 Spatially 3-D plasma *kinetic* models. These will represent the full fluid model produced by the 5-year NEPTUNE project, incorporating features of 2-D fluid and *kinetic* work in a 3-D code.

3-1 2-D particle-based model of neutral gas & impurities with critical physics. This will be a $2d3v$ code (ie. spatially 2-D distribution of particles with 3 velocity components) designed from the outset to interact with a high-order finite-element fluid model of plasma. It gives an opportunity to check out ideas on optimal usage of particles.

3-2 2-D moment-based model of neutral gas & impurities. Constructing a 2-D fluid code of neutral gas from the Nektar++ software should be a valuable educational exercise, whilst providing scope for cross-validating the 2-D particle model.

3-3 Interaction with 2-D plasma model when available. Building on the 1-D multispecies fluid work, the challenge here is to incorporate in the fluid code of Proxyapp PA2-6, particle effects from PA3-1, which will in the higher dimensional space be more subject to lack of numerical resolution or 'noise'. Should PA3-3 be accelerated, it could usefully treat both plasma and neutrals via particle models.

3-4 3-D model of neutral gas & impurities. This is now at full dimensional complexity, incorporating selected ideas on optimal usage of particles.

3-5 Interaction with 3-D plasma model. This will represent the full model produced by the 5-year NEPTUNE project, a coupling of fluid and *kinetic* software developed under the FM-WP2 work-package as PA2-8, incorporating features of Proxyapps 3-1 to 3-4, and allowing for additional input from PA3-6.

3-6 Staged introduction of additional neutral gas/impurity physics. It is expected that the NEPTUNE community will join in to supplement the software with a wide-ranging capability to treat a wide range of additional nuclear, atomic and molecular effects.

2 Braginskii coefficients

Braginskii's transport coefficients are widely used in tokamak edge modelling. Object-oriented Fortran code to compute the Braginskii coefficients is available at
`https://github.com/wayne-arter/smardda-misc.git`.

2.1 General

Note that $k_BT(\text{units of } K) = |e|T(\text{units of } eV)$ where k_B is Boltzmann's constant and $|e|$ is the absolute value of the charge on the electron. Otherwise suffix B denotes a quantity from the Plasma Formulary [6]. See also Braginskii's paper [7]. The subsequent corrections by Epperlein and Haines, and by Mikhailovski and Tsypin are not relevant to this work.

In a magnetic field, the direction of which is given by unit vector $\mathbf{b}$, Goedbloed and Poedts [8] define three auxilliary vectors for a vector $\mathbf{v}$, viz.

$$\mathbf{v}_\parallel = \mathbf{b}(\mathbf{b}\cdot\mathbf{v}),\ \ \mathbf{v}_\wedge = \mathbf{b}\times\mathbf{v} \text{ and } \mathbf{v}_\perp = (\mathbf{b}\times\mathbf{v})\times\mathbf{b} \tag{1}$$

If $\mathbf{v} = (v_1, v_2, v_\parallel)$ and $\mathbf{b}$ is aligned with the 3-axis in a Cartesian coordinate system, then

$$\mathbf{v}_\parallel = (0,0,v_\parallel),\ \ \mathbf{v}_\wedge = (-v_2, v_1, 0) \text{ and } \mathbf{v}_\perp = (v_1, v_2, 0) \tag{2}$$

It may be shown that a tensor $\mathcal{T}$ which is symmetric under rotation about $\mathbf{b}$ has the form (in Cartesians)

$$\mathcal{T} = \begin{pmatrix} \mathcal{T}_\perp & -\mathcal{T}_\wedge & 0 \\ \mathcal{T}_\wedge & \mathcal{T}_\perp & 0 \\ 0 & 0 & \mathcal{T}_\parallel \end{pmatrix} \tag{3}$$

so that

$$\mathcal{T}\cdot\mathbf{v} = \mathcal{T}_\parallel\mathbf{v}_\parallel + \mathcal{T}_\wedge\mathbf{v}_\wedge + \mathcal{T}_\perp\mathbf{v}_\perp \tag{4}$$

2.2 Conduction, Viscous and Resistive Coefficients

The electron parallel thermal conductivity in the Braginskii theory is given as [6]

$$\kappa^e_{B\parallel} = 3.2\frac{Nk_BT_e}{m_e}\tau_e \tag{5}$$

a formula valid in either cgs or SI units, where τ_e is the electron relaxation time (measured in seconds), defined below. The notation is standard, with N the number density of electrons, approximately the same as the number density of ions, m_e the electron mass, and $T_\alpha, \quad s = i, e$ the temperature of species α. The perpendicular electron thermal conductivity satisfies similarly

$$\kappa^e_{B\perp} = 4.7 \frac{N k_B T_e}{m_e} \tau_e \cdot \frac{1}{(\omega_{ce}\tau_e)^2} \tag{6}$$

where the electron cyclotron frequency

$$\omega_{ce} = \frac{e}{m_e} \cdot B \tag{7}$$

Equivalent expressions for ions are

$$\kappa^i_{B\parallel} = 3.9 \frac{N k_B T_i}{m_i} \tau_i \tag{8}$$

$$\kappa^i_{B\perp} = 2 \frac{N k_B T_i}{m_i} \tau_i \cdot \frac{1}{(\omega_{ci}\tau_i)^2} \tag{9}$$

where the ion cyclotron frequency

$$\omega_{ci} = \frac{ZeB}{m_i} = \frac{e}{m_p} \cdot \frac{ZB}{A} \tag{10}$$

where Z is the charge state of the ion and A its atomic mass. The definitions above have to be interpreted in the context of the equations given in [6], so that thermal diffusivities are obtained by dividing by $3n_\alpha/2$ where $\alpha = i, e$ is the species index. It is also convenient to introduce the dimensionless factors

$$x_e = \omega_{ce}\tau_e \tag{11}$$

$$x_i = \omega_{ci}\tau_i \tag{12}$$

Kinematic viscosities in the Braginskii theory may be taken as

$$\nu^e_\parallel = 0.73 N k_B T_e \tau_e / (N m_e) = 0.73 \frac{k_B T_e}{m_e} \tau_e \tag{13}$$

$$\nu^e_\perp = 0.51 N k_B T_e \tau_e / (N m_e) \frac{1}{x_e^2} = 0.51 \frac{k_B T_e}{m_e} \tau_e \frac{1}{x_e^2} \tag{14}$$

$$\nu^i_\parallel = 0.96 N k_B T_i \tau_i / (N m_i) = 0.96 \frac{k_B T_i}{m_i} \tau_i \tag{15}$$

$$\nu^i_\perp = 0.3 N k_B T_i \tau_i / (N m_i) \frac{1}{x_i^2} = 0.3 \frac{k_B T_i}{m_i} \tau_i \frac{1}{x_i^2} \tag{16}$$

Key quantities in the calculation of all these terms are τ_α, $\alpha = i, e$. The first step in their calculation is to convert their formulas, usually given in cgs, to SI units, giving

$$\tau_e = 6\sqrt{2\pi^3} \frac{\epsilon_0^2 \sqrt{m_e}}{e^4} \frac{(k_B T_e)^{3/2}}{Z^2 N \Lambda} = 3.44 \times 10^{-7} \frac{(T_e)^{3/2}}{Z^2 (N/10^{18}) \Lambda} \tag{17}$$

$$\tau_i = 12\sqrt{\pi^3}\frac{\epsilon_0^2\sqrt{m_p}}{e^4}\frac{(k_B T_i)^{3/2}\sqrt{A}}{Z^4 N\Lambda} = 2.09\times 10^{-5}\frac{(T_i)^{3/2}\sqrt{A}}{Z^4(N/10^{18})\Lambda} \tag{18}$$

where the notation is standard, except possibly the use of Λ for the Coulomb logarithm. The above check with expressions in Wesson [9, § 14]. Note that $Z^2\tau_i$ differs from τ_e in being larger by a factor of $\sqrt{2m_i/m_e} \approx 60\sqrt{A}$ (also substituting T_i for T_e is necessary). The factors in Z are taken from the original Braginskii paper [7].

It follows that the x_α factors may be conveniently written

$$x_e = 6.05\times 10^4\frac{(T_e)^{3/2}B}{Z^2(N/10^{18})\Lambda} \tag{19}$$

$$x_i = 1997\frac{(T_i)^{3/2}B}{Z^3(N/10^{18})\sqrt{A}\Lambda} \tag{20}$$

The large coefficients in Equations(19) and (20) explain why classical transport is so anisotropic.

Substituting the explicit expression for τ_e in Equations(5) and (8) gives respectively, the thermal parallel diffusivities are

$$\kappa_{e\|} = 13\sqrt{2\pi^3}\frac{1}{\sqrt{m_e}}\frac{\epsilon_0^2}{e^4}\cdot\frac{(k_B T_e)^{5/2}}{Z^2 N\Lambda} \tag{21}$$

$$\kappa_{i\|} = 16\sqrt{\pi^3}\frac{1}{\sqrt{m_p}}\frac{\epsilon_0^2}{e^4}\cdot\frac{(k_B T_i)^{5/2}}{Z^4 N\Lambda\sqrt{A}} \tag{22}$$

and the ratios are

$$x_e = \frac{6\sqrt{2\pi^3}\epsilon_0^2}{\sqrt{m_e}e^3}\cdot\frac{(k_B T_e)^{3/2}B}{Z^2 N\Lambda} \tag{23}$$

$$x_i = \frac{12\sqrt{\pi^3}\epsilon_0^2}{\sqrt{m_p}e^3}\cdot\frac{(k_B T_i)^{3/2}B}{Z^3 N\Lambda\sqrt{A}} \tag{24}$$

An expression for the perpendicular ion conductivity, maintaining the fixed physical factors is of interest

$$\kappa_{i\perp} = \frac{e^2\sqrt{m_p}}{9\sqrt{\pi^3}\epsilon_0^2}\cdot\frac{Z^2 N\Lambda\sqrt{A}}{(k_B T_i)^{1/2}B^2} \tag{25}$$

Assuming T_i is measured in eV, and N in units of $10^{18}\,\mathrm{m}^{-3}$, then

$$\kappa_{i\perp} = 6.67\times 10^{-4}\cdot\frac{Z^2(N/10^{18})\Lambda\sqrt{A}}{(T_i)^{1/2}B^2}\ \ m^2 s^{-1} \tag{26}$$

and

$$\kappa_{e\perp} = 5.26\times 10^{-5}\cdot\frac{Z^2(N/10^{18})\Lambda}{(T_e)^{1/2}B^2}\ \ m^2 s^{-1} \tag{27}$$

The plasma resistivity is taken as

$$\eta = \eta_B/\mu_0 = \frac{0.51\sqrt{m_e}e^2}{6\sqrt{2\pi^3}\mu_0\epsilon_0^2}\cdot\frac{Z\Lambda}{(k_B T_e)^{3/2}} \tag{28}$$

Assuming T_e is measured in eV, then

$$\eta = \eta_B/\mu_0 = 41.9\cdot\frac{Z\Lambda}{(T_e)^{3/2}}\ \ m^2 s^{-1} \tag{29}$$

2.3 Prandtl Numbers

The above expressions (except for the resistivity) apply strictly only when there are separate equations for ion and electron transport, so decisions have to be taken about how to combine the transport coefficients to treat the plasma as a single fluid. For the thermal transport, since pressures $p_e \approx p_i$, it is sufficient to add the κ_α. However, the values for ions and electrons are so disparate because $m_p \gg m_e$ that one or other might be neglected, assuming B is of order unity (in Tesla) and $T_e \approx T_i$, thus $\kappa_{e\|} \gg \kappa_{i\|}$ and hence $\kappa_\| \approx \kappa_{e\|}$, since

$$\left(\frac{x_i}{x_e}\right)^2 = \frac{2m_e}{Z^2 A m_p}\left(\frac{T_i}{T_e}\right)^3 \tag{30}$$

It also follows that

$$\frac{\kappa_{e\perp}}{\kappa_{i\perp}} = 0.078\left(\frac{T_i}{T_e}\right)^{1/2}\frac{1}{\sqrt{A}} \tag{31}$$

thus $\kappa_\perp \approx \kappa_{i\perp}$. There is the caveat that if T_i is approximately spatially constant radially, then $\kappa_{e\perp}$ might become relevant.

As for viscosity, since the ion momentum is so much greater than the electron momentum, then $\nu \approx \nu^i$.

For interchange motions where flows are perpendicular to the field, take $\kappa = \kappa_{i\perp}$, then on the *Cambridge* definition, the magnetic Prandtl number is

$$\zeta = \frac{\eta}{\kappa_{i\perp}} = \frac{0.765}{\sqrt{2}}\frac{1}{\mu_0}\sqrt{\frac{m_e}{m_p}}\cdot\frac{B^2}{ZN\sqrt{A}}\frac{(k_B T_i)^{1/2}}{(k_B T_e)^{3/2}} \tag{32}$$

which evaluates as (T_α in eV, N in units of $10^{18}\,\mathrm{m}^{-3}$)

$$\zeta = \frac{\eta}{\kappa_{i\perp}} = 62\,700\cdot\frac{B^2}{Z(N/10^{18})\sqrt{A}}\frac{(T_i)^{1/2}}{(T_e)^{3/2}} \tag{33}$$

It may be argued that it is more appropriate to use the 'anomalous' value of $1\,m^2 s^{-1}$, in which case Equation (29) without units gives the 'Cambridge' magnetic Prandtl number.

The usual Prandtl number is

$$\sigma = \frac{\nu_{i\perp}}{\kappa_{i\perp}} = 0.23 \tag{34}$$

Note that P.H.Roberts [10] defines the magnetic Prandtl number as $\nu/\eta = \sigma/\zeta$, and his definition is more widely used.

3 System 2-1: 2-D model of anisotropic heat transport

The model for time evolution of the temperature field T is thermal diffusion, which in a plasma gives

$$\frac{3}{2}N\frac{\partial T}{\partial t} = \nabla \cdot \kappa \nabla T \tag{35}$$

where the thermal conductivity tensor is κ. (Compare the model for a solid

$$\rho_m c_p \frac{\partial T}{\partial t} = \nabla \cdot k_c \nabla T \tag{36}$$

where the thermal conductivity tensor is k_c, ρ_m is the mass density of the medium and c_p is its specific heat at constant pressure, implying that the thermal diffusivity tensor is $\kappa = k_c/\rho_m c_p$.) Introducing vector components as in Section 1, thermal diffusion in a plasma after Braginskii is thus

$$\frac{3}{2}N\frac{\partial T}{\partial t} = \nabla \cdot \left(\kappa_\parallel \mathbf{b}[\mathbf{b}.\nabla T] + \kappa_\perp(\nabla T - \mathbf{b}[\mathbf{b}.\nabla T]) + \kappa_\wedge \mathbf{b} \times \nabla T\right) \tag{37}$$

Henceforth, the 'wedge' transport ie. in due to the term in $\kappa_\wedge$ is neglected for the reason that it may be rearranged to give a convection-like term, via the identity

$$\nabla \cdot \kappa_\wedge \mathbf{b} \times \nabla T = \nabla \cdot (\mathbf{u}_\wedge T) \tag{38}$$

where

$$\mathbf{u}_\wedge = \nabla \times (\kappa_\wedge \mathbf{b}) \tag{39}$$

(In any event, if $\kappa_\wedge$ is a function purely of T, and $\nabla \cdot \mathbf{b} = \mathbf{0}$, then the terms in Equation (38) vanish.)

Expressions for $\kappa_\perp$ and $\kappa_\parallel$ for the different species are given in Section 2.2, where they incorporate the factor $\frac{3}{2}N$, ie. $\kappa_{(\perp,\parallel)}/(\frac{3}{2}N) = \kappa_{(\perp,\parallel)e,i}$.

3.1 Test Cases

The aim of the work is to calculate in a series of calculations that increasingly approach the realistic model, the magnitude of the spurious numerical diffusion perpendicular to the magnetic field direction $\mathbf{b}$. The main interest concerns how much diffuses in the plasma, not the solid surface, even though the deposition of power is on the surface, reason: all sorts of complicated extra physics come into play in the plasma especially near surfaces.

3.1.1 Starting Case

For the 2-D test case illustrated in Figure 1, it is suggested that $\kappa_\perp = 0$ so that any perpendicular diffusion is numerical in origin. Given this, the problem can be analysed using any spatial scale and any convenient $\kappa_\parallel$. However an order of magnitude estimate for tile dimensions is one metre, discharge timescale is one second upwards. For plasma properties assume $N = 10^{18}\,\mathrm{m}^{-3}$, $T_i = T_e = 10\,\mathrm{eV}$, $Z = A = 1$, $B = 3\,\mathrm{T}$ and solid temperatures say $500^o\,\mathrm{C}$.

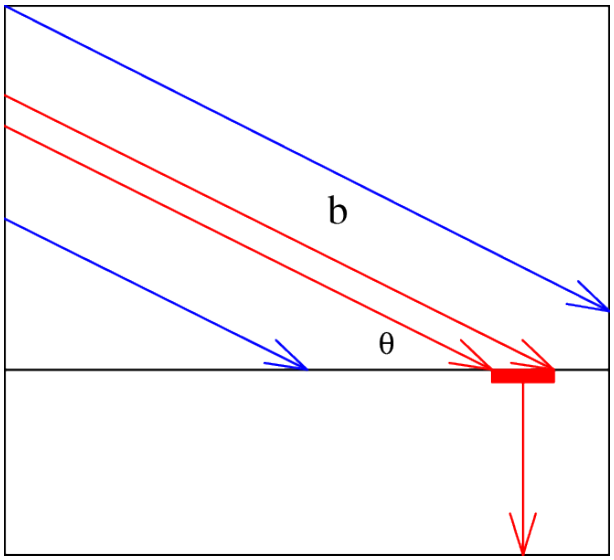

Figure 1: Sketch of the test configuration, showing fieldlines in direction $\mathbf{b}$ and the boundary between anisotropic conductor and perfect insulator.

In Figure 1, $T = T_0 > 0$ over the interval on the left hand boundary that is connected by field in direction $\mathbf{b}$ with the thick red line, elsewhere on the blue fieldlines, $T = 0$. The red region lies on a black line which denotes the boundary between anisotropic conductor and perfect insulator. The exact steady-state solution has $T = constant$ along fieldlines, but numerical diffusion will result in non-zero T in the region of blue fieldlines. The relative size of this numerical diffusion must be estimated as a function of incidence angle θ, where interest attaches to small $\theta \leq 2^o$.

3.1.2 Intermediate Case

To test curvature effects the whole 2-D domain of Figure 1 could be distorted by conformal mapping (which preserves angles).

3.1.3 Realistic Case

This needs to be 3-D and involve JET divertor tile descriptions derived from the output of the CAD design tool, together with information describing the magnetic field as a function of position, which will be supplied. The magnetic equilibrium may be supplied analytically after Solovev, but the usual input is as an .eqdsk file. The EQDSK G format is a “non-standard” standard for solutions $\psi(R, Z), p(\psi), F(\psi)$ of the Grad-Shafranov equation, where ψ is the magnetic flux and (R, Z) are cylindrical coordinates in planes normal to the toroidal direction. The functions p and F give the variation of the pressure and toroidal field respectively. The basic standard for EQDSK G may be found at: `https://fusion.gat.com/theory/Efitgeqdsk` (which may be password-protected) or else at `https://w3.pppl.gov/ntcc/TORAY/G_EQDSK.pdf` The flux $\psi(R, Z)$ is sampled at uniformly spaced points on a direct product grid, for which the .eqdsk header defines the mesh-size,

as well as other useful information, such as the flux on axis and at boundary. Unfortunately the strict EQDSK G standard uses a Fortran format that does not require spaces between samples, hence there are many variants for languages that cannot handle this situation, that have introduced other features such as mistakes in field helicity, factors of 2π in the flux, etc. Routines that calculate magnetic field $\mathbf{B}$ using cubic spline interpolation could be made available. It would be desirable for the output of System 2-2 to be used.

3.1.4 Extended Case

An extended test would allow for heat transfer in the solid surface sketched at bottom of Figure 1, taking say thermal diffusivity for Tungsten $\kappa \approx 3 \times 10^{-5}\,\mathrm{m}^2\,\mathrm{s}^{-1}$.

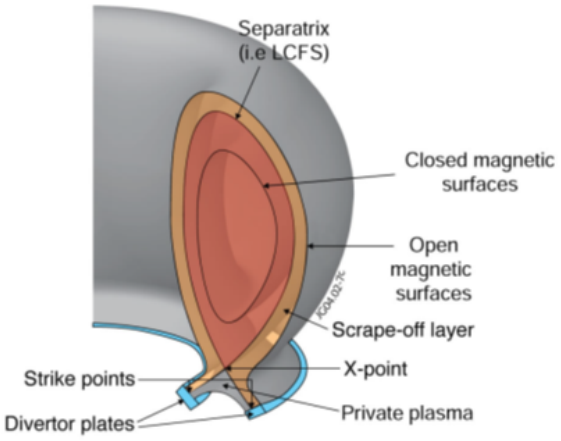

Figure 2: Sketch of the test configuration, showing tokamak cross-section and the boundary of the Last Closed Flux Surface (LCFS).

4 System 2-2: 2-D elliptic solver in complex geometry

The geometry will be representative of a tokamak cross-section, possibly omitting the region containing the central hot plasma, so that topologically it will be at most as complex as an annulus (one-hole). Figure 2 provides an example. The Last Closed Flux Surface (LCFS) may be parameterised by arc-length in the cross-sectional plane of projection.

The elliptic equations to be considered now follow.

4.1 Simplified Grad-Shafranov equation

This elliptic equation is a simplified version of the Grad-Shafranov equation, see [11]

$$R^2 \nabla \cdot \frac{1}{R^2} \nabla \psi = -2\mu_0 R J_\phi \tag{40}$$

where ψ is the poloidal magnetic flux and (R, Z) are cylindrical coordinates in planes normal to the toroidal direction ϕ, with the toroidal current

$$J_\phi = R\frac{dp(\psi)}{d\psi} + \frac{I}{\mu_0 R}\frac{dI(\psi)}{d\psi} + J_{ext}(R, Z) \tag{41}$$

The functions p and I give the variation as functions of ψ of the pressure and toroidal field respectively, and $J_{ext}(R, Z)$ may be produced in several ways, of which the commonest is by poloidal field circuits, ie. localised current sources in cross-section. Note that the operator in Equation (40) simplifies to

$$\frac{\partial^2}{\partial R^2} - \frac{1}{R}\frac{\partial}{\partial R} + \frac{\partial^2}{\partial Z^2} \tag{42}$$

which implies that mathematically, ψ satisfies a steady-state 2-D advection-diffusion equation corresponding to unit diffusivity in the flow $u_R = 1/R$.

To provide the simple test case, take $J_\phi = J_{ext}$ only with localised current sources. The boundary conditions are $\psi = 0$ on the LCFS and $\psi \propto 1/\sqrt{(R^2 + Z^2)}$ as $R,\ Z \to \infty$.

Note that the Grad-Shafranov equation has been solved using spectral elements by others, eg. Sovinec [3].

4.2 Simplified non-Boussinesq vorticity equation

A simplified version of the non-Boussinesq vorticity equation to be solved for the scalar field $\Phi(R, Z)$ in cylindrical polar coordinates (R, Z) is

$$\nabla_\perp \cdot \left(\frac{1}{B^2} \nabla_\perp \Phi \right) = n \tag{43}$$

where $B = |\mathbf{B}|$ is the amplitude of the imposed magnetic field, density n acts as a source term, and the elliptic is to be solved for Φ, subject to boundary conditions $\Phi = 0$. The operator $\nabla_\perp$, ignoring the components of magnetic field directed within the (R, Z) plane, reduces to the usual gradient ∇ in cylindrical polars of axisymmetric fields, hence mathematically Equation (43) is equivalent to Equation (40).

n will be set so that $n = n_0(s_i)$ on the boundaries, where arc-length s_i parameterises the inner boundary if $i = 1$ and the outer if $i = 2$. n and $|B|$ will be specified functions of (R, Z) that capture features of the number density n distribution and magnetic field intensity distribution expected in a tokamak, Ideally $|B|$ would represent a solution of the Grad-Shafranov equation from Section 4.1.

5 System 2-3: 1-D fluid solver with simplified physics but with UQ and realistic boundary conditions

5.1 Plasma Equations

It is assumed that the single spatial dimension of the problem corresponds to the arc length distance along a fieldline. Starting from the two-fluid model of Braginskii [7], a set of equations resembling those of classical (compressible) hydrodynamics may be derived by summing Braginskii's equations for number density, momentum and energy. Using the notation of ref [12], introducing $T_d = T_i + T_e$, neglecting the stress tensor terms (implicitly setting $\delta p_i = 0$), and assuming B is independent of time, the resulting system is

$$U_d \frac{\partial}{\partial t}(N/B) + \frac{\partial}{\partial s}(NU/B) = \frac{L_s S^n}{B} \tag{44}$$

$$U_d \frac{\partial}{\partial t}(NU/B) + \frac{\partial}{\partial s}(NU^2/B) = -\frac{1}{m_i B}\frac{\partial}{\partial s}(P_i + P_e) + \frac{L_s S^u}{m_i B} \tag{45}$$

$$U_d \frac{\partial}{\partial t}\left(\frac{3}{2}(NkT_d/B) + \frac{1}{2}(NU^2/B)\right) + \tag{46}$$

$$\frac{\partial}{\partial s}\left(\frac{5}{2}(NUkT_d/B) + \frac{1}{2}(NU^3/B)\right) = -\frac{1}{m_i B}\frac{\partial}{\partial s}(q_i + q_e) + \frac{L_s(S_i^E + S_e^E)}{m_i B} \tag{47}$$

where

$$L_s = \frac{\partial s_\parallel}{\partial s} \tag{48}$$

$U_d = L_s/t_0$ is a speed measuring the importance of the transient term, s parameterises distance along the fieldline, and some variables from [12] have been promoted to capitals to indicate that they retain their physical dimensions. For the case of a fieldline connecting two walls at $s = \pm L$,

$$s_\parallel = L(2s - 1) \tag{49}$$

and so $L_s = 2L$. The constant k is such that

$$k = \frac{k_B}{m_i} \text{ or } k = \frac{|e|}{m_i} \tag{50}$$

where k_B is Boltzmann's constant and $|e|$ is the unit of charge, depending whether T is measured in Kelvin or eV. Note that in adding Eqs.(3) and (4) of [12], equipartition and collision terms cancel to give Equation (47). The perfect gas equation of state will be assumed, so that

$$\frac{p_i + p_e}{m_i} = NkT \tag{51}$$

The boundary conditions are that $|U| = |M_s| C_S$ at $s = 0, 1$ where the sound speed

$$C_S = \sqrt{kT_d} \tag{52}$$

and $|M_s|$ is the Mach number, since M_s will be allowed to take either sign. Normally $|M_s| = 1$ so that $M_0 = -1$ and M_1=1 where the subscript corresponds to value of s. The combined energy flux at each boundary has

$$|Q_{\parallel}| = m_i C_S N(\delta_e k T_e + \delta_i k T_i) \approx m_i C_S N \delta k T_d \tag{53}$$

if $\delta \approx \delta_e \approx \delta_i$. For definiteness, $\delta = \frac{1}{2}(\delta_e + \delta_i)$ will be assumed.

5.2 Fluid Equations with Sources

It is convenient to replace the source terms in Equations(44)– (47) by equivalent fluxes

$$F^n(s) = \int_0^s \frac{S^n}{B} ds_{\parallel} \tag{54}$$

$$F^u(s) = \int_0^s \frac{S^u}{m_i B} ds_{\parallel} \tag{55}$$

$$F^E(s) = 2\int_0^s \frac{S_i^E + S_e^E}{m_i B} ds_{\parallel} \tag{56}$$

and write

$$F^Q(s) = -\frac{1}{m_i B}(q_i + q_e) \tag{57}$$

The convention with respect to limits of integration is that they are specified in terms of parameterised length and to use the appropriate relation for $s_{\parallel}(s)$, thus in the case of Equation (49), the lower limit of 0 corresponds to $s_{\parallel}(s) = -L$. The forms the sources take are discussed below in Section 5.3. Observing the identity

$$\frac{1}{B}\frac{\partial}{\partial s} B n_B k T_d = \frac{\partial}{\partial s}(n_B k T_d) + n_B k T_d \frac{\partial}{\partial s}(\ln B) \tag{58}$$

and the frequent appearance of $n_B = N/B$, the governing equations in dimensional form become

$$U_d \frac{\partial}{\partial t} n_B + \frac{\partial}{\partial s}(n_B U) = \frac{\partial}{\partial s} F^n \tag{59}$$

$$U_d \frac{\partial}{\partial t}(n_B U) + \frac{\partial}{\partial s}(n_B U^2) = -\frac{\partial}{\partial s}(n_B k T_d) + \frac{\partial}{\partial s} F^u \tag{60}$$

$$U_d \frac{\partial}{\partial t}\left(\frac{3}{2}(n_B k T_d) + \frac{1}{2}(n_B U^2)\right) + \tag{61}$$

$$\frac{\partial}{\partial s}\left(\frac{5}{2}(n_B U k T_d) + \frac{1}{2}(n_B U^3)\right) = -\frac{\partial}{\partial s} F^Q + \frac{1}{2}\frac{\partial}{\partial s} F^E \tag{62}$$

where the derivative of $\ln B$ has been neglected. The boundary conditions on U are unchanged and

$$|Q_{\parallel}| = m_i C_S n B \delta k T_d \tag{63}$$

The Equations(59)– (62) together with boundary condition Equation (63) are in units such that equivalence may easily be established with those of ref [12] (by setting $U_d = 1$ and identifying s with $s_{\parallel}$). To proceed, it may be helpful to make the preceding system of equations dimensionless, by scaling n_B with respect to N_0/B_0, kT_d with respect to kT_0, U with respect to C_0 and B with respect to B_0. If the subscript 0 corresponds to the value of a variable at $s = 0$, then it is convenient to take $C_0 = \sqrt{kT_0}$. The resulting system may be deduced from the coupled model in Section 5.4.

5.3 Explicit Sources

The above work concentrates on the case where the source terms are regarded as given, however it is worth describing the form of the additional sources that may be at least locally important. From ref [12], the plasma sources are given by (with the convention that suffix 'n' denotes neutral species)

$$
\begin{aligned}
S^n &= N_n N\langle\sigma v\rangle_{ION} - N^2\langle\sigma v\rangle_{REC} + S^n_\perp && (64)\\
S^u &= N_n N\langle\sigma v\rangle_{ION} U_n - N^2\langle\sigma v\rangle_{REC} U + N_n N(U_n - U)\langle\sigma v\rangle_{CX} && (65)\\
S^E &= S^E_i + S^E_e && (66)\\
&= N_n N\langle\sigma v\rangle_{ION}(\frac{3}{2}k_B T_n + \frac{1}{2}m_n U_n^2 - k_B I_H) && (67)\\
&- N^2\langle\sigma v\rangle_{REC}(\frac{3}{2}k_B T_i + \frac{1}{2}m_i U^2)\\
&+ N_n N\langle\sigma v\rangle_{CX}\left(\frac{3}{2}k_B(T_n - T_i) + \frac{1}{2}m_n(U_n^2 - U^2)\right)\\
&- N_n N k_B Q_H + S^E_{\perp i} + S^E_{\perp e}
\end{aligned}
$$

Here suffix $\perp$ denotes the effectively given source terms arising from cross-field contributions, suffices ION, REC and CX denote respectively cross-sections $\langle\sigma v\rangle$ for ionisation, recombination and charge-exchange reactions, I_H is the Hydrogen reionisation potential, and Q_H is the cooling rate due to excitation.

Since the sources appear in the analysis primarily as integrals starting at $s = 0$, study of Equations(64)– (66) concentrates on this region, where plasma velocity $U < 0$ and neutral velocity $U_n > 0$ with the two having approximately the same magnitude. There, Equation (64) has only one negative term, due to recombination, but from the cross-section data in ref [12], this could dominate only below 2 eV. All terms in Equation (65) are positive near $s = 0$ as the two velocities reinforce. Equation (66) contains two terms which are always negative and an ionisation term which is also negative below $I_H/2 \approx 7$ eV, thus for example, the cross-field source terms $S_{\perp i,e}$ must be positive for $S^E > 0$.

The sources of neutrals may be deduced from the ionisation and charge-exchange terms in Equations(64)– (66), viz.

$$
\begin{aligned}
S^n_n &= -N_n N\langle\sigma v\rangle_{ION} + S^n_{\perp,n} && (68)\\
S^u_n &= -N_n N\langle\sigma v\rangle_{ION} U_n - N_n N(U_n - U)\langle\sigma v\rangle_{CX} S^u_{\perp,n} && (69)\\
S^E_n &= -N_n N\langle\sigma v\rangle_{ION}(\frac{3}{2}k_B T_n + \frac{1}{2}m_n U_n^2 - k_B I_H) && (70)\\
&- N_n\langle\sigma v\rangle_{CX}\left(\frac{3}{2}k_B(T_n - T_i) + \frac{1}{2}m_n(U_n^2 - U^2)\right) && (71)\\
&+ S^E_{\perp n} && (72)
\end{aligned}
$$

The $S_{\perp,n}$ terms are hard to quantify, but if these are neglected, it is clear that $S^n_n < 0$ and $S^u_n < 0$ is the obverse of the positive plasma sources. Similarly it is likely that $S^E_n < 0$ if $S^E > 0$

5.4 Coupled System

Working within the flux-tube geometry, the equations for neutral transport take the same form as those used for plasma above, however the boundary conditions are different. They become at $s = 0$, supposing that $\mathsf{T}(0) = \tau^2 T_0$ and masses $m_n = m_i$, in dimensionless units,

$$\mathsf{n} = R_2 = \frac{R}{\tau}|M_0| \tag{73}$$

$$\mathsf{u} = -\tau \tag{74}$$

$$\mathsf{T} = \tau^2 \tag{75}$$

where n, u and T are neutral density, temperature and density made dimensionless with respect to the same N_0 and T_0 as the corresponding plasma quantities, and R is the recycling coefficient. Note the usage of a sans-serif font to denote dimensionless neutral species quantities, and that n does not however include a factor of $\tilde{b} = B/B_0$, as the neutral flux is not constrained by the flux tube.

A system explicitly modelling the coupling between plasma and neutrals may be derived by making non-dimensionless the sources set out in Section 5.3, and assuming $m_n = m_i$, $\mathsf{T} = T_i = \tau^2 T$, giving 5 equations for the evolution of plasma density, velocity, total temperature, neutral density and neutral velocity:

$$\epsilon_r \frac{\partial}{\partial t} n + \frac{\partial}{\partial s}(nu) = \sigma_I n \mathsf{n} + \frac{\partial}{\partial s} f^n \tag{76}$$

$$\epsilon_r \frac{\partial}{\partial t}(nu) + \frac{\partial}{\partial s}(nu^2 + nT) = \sigma_I n \mathsf{nu} + \sigma_c n \mathsf{n}(\mathsf{u} - u) + \frac{\partial}{\partial s} f^u \tag{77}$$

$$\begin{aligned} \epsilon_r \frac{\partial}{\partial t}\left((g-2)nT + nu^2\right)) &+ \\ \frac{\partial}{\partial s}\left(gnuT + nu^3\right) &= \sigma_I n \mathsf{n}(3[\tau^2 T - T_H] + \mathsf{u}^2) + \sigma_C n \mathsf{n}(\mathsf{u}^2 - u^2) \\ &- \sigma_E n \mathsf{n} + \frac{\partial}{\partial s} f^E \end{aligned} \tag{78}$$

$$\epsilon_r \frac{\partial}{\partial t}\mathsf{n} + \frac{\partial}{\partial s}(\mathsf{nu}) = -\sigma_I n \mathsf{n} \tag{79}$$

$$\epsilon_r \frac{\partial}{\partial t}(nu) + \frac{\partial}{\partial s}(\mathsf{nu}^2 + \mathsf{n}\tau^2 T) = -\sigma_I n \mathsf{nu} - \sigma_c n \mathsf{n}(\mathsf{u} - u) \tag{80}$$

where $\epsilon_r = L_s/(t_0 C_0)$ with t_0 a characteristic timescale. The reaction cross-sections are made dimensionless by division by $C_0/(L_s N_0)(\simeq 3.1 \times 10^{-16}\, m^3 s^{-1}$ for representative parameter values), so that

$$\sigma_I = \frac{\langle \sigma v \rangle_{ION}}{C_0/L_S N_0} \tag{81}$$

$$\sigma_C = \frac{\langle \sigma v \rangle_{CX}}{C_0/L_S N_0} \tag{82}$$

$$\sigma_E = \frac{2Q_H}{C_0 T_0/L_S N_0} \tag{83}$$

$$T_H = \frac{2I_H}{3T_0} \simeq 9/T_0 (\text{in eV}) \tag{84}$$

where I_H and Q_H are as defined in ref [12].

It is of interest to allow a stochastic ('turbulent') contribution to the terms $f^{n,u,E}$.

5.5 Uncertainty Quantification

Polynomial chaos (PC) refers to a situation whereby probability functions are expanded as Hermite polynomials, and generalised Polynomial chaos (gPC) to expansions using Hermite and other polynomial sets $\{\Psi_j(\xi)\}$ [13]. Thus for example, suppose θ to denote a random event, and the number density field to have the following representation in terms of a finite number P of such modes.

$$n(\mathbf{x}, t, \theta) = \sum_{j=0}^{P} n_j(\mathbf{x}, t)\Psi_j\left(\boldsymbol{\xi}(\theta)\right) \tag{85}$$

where $\{n_j(\mathbf{x}, t)\}$ is the set of deterministic coefficients of the "random trial basis", ie. the set $\{\Psi_j\left(\boldsymbol{\xi}(\theta)\right)\}$ where $\boldsymbol{\xi}(\theta)$ is a multi-dimensional random variable with a specific probability distribution as a function of the random parameter $0 \leq \theta \leq 1$. Note that the Ψ_j are the set of multi-dimensional Hermite polynomials if $\boldsymbol{\xi}$ is a vector. Typically but not necessarily the $\boldsymbol{\xi}(\theta)$ will be Gaussians. Expressions like Equation (86) may be substituted into a governing equation of say advection type for n, and the result simplifies because spatial operators do not interact with the random variables, then taking the inner product with $\Psi_k\left(\boldsymbol{\xi}(\theta)\right)$ yields

$$\frac{\partial n_k}{\partial t} + \sum_{i=0}^{P}\sum_{j=0}^{P} e_{ijk}\frac{\partial u_i n_j}{\partial s} = 0 \tag{86}$$

where e_{ijk} is a weighted integral of triple products of Ψ_i. Hence there are now P equations instead of one for n.

There is an alternative treatment by Polynomial Chaos Expansion (PCE) which is non-intrusive and therefore preferred. It relies on projecting a set of randomly selected solutions onto a Hermite or similar basis, see further description in ref [14, end § 2.1.1].

6 System 2-4: Spatially 1-D plasma model incorporating velocity space effects

The following simple model is after Taitano et al [15, 16]

$$\begin{aligned} \frac{\partial f_e}{\partial t} + v_{ex}\frac{\partial f_e}{\partial x} + \frac{q_e}{m_e}\mathbf{E}\cdot\frac{\partial f_e}{\partial \mathbf{v}} &= 0 \\ \frac{\partial f_i}{\partial t} + v_{ix}\frac{\partial f_i}{\partial x} + \frac{q_i}{m_i}\mathbf{E}\cdot\frac{\partial f_i}{\partial \mathbf{v}} &= 0 \\ \epsilon_0\frac{\partial \mathbf{E}}{\partial t} + \sum_\alpha q_\alpha n\mathbf{u}_\alpha - \overline{\sum_\alpha q_\alpha n\mathbf{u}_\alpha} &= 0 \end{aligned} \tag{87}$$

Equations 87 are the electron and ion Vlasov equations and Ampere's equation respectively. The quantities m_e, m_i, f_e, f_i, $\mathbf{v}_e$, $\mathbf{v}_i$, q_e, q_i, $\mathbf{E}$, ϵ_0, and $n\mathbf{u}_\alpha$ are the electron and ion masses, electron and ion distribution functions, electron and ion velocities, electron and ion charges, the electric field, permeability constant of vacuum, and the momentum of species $\alpha = i, e$, respectively. Note that Equation (87)represents a generalisation of the system in ref [15], where for vector quantities, the x-component is always implied, in the usual notation the original system is $1d1v$ rather than $1d3v$ as above, where particles move according to

$$\begin{aligned} \frac{dx}{dt} &= v_{\alpha x} \\ \frac{d\mathbf{v}_\alpha}{dt} &= \frac{q_\alpha}{m_\alpha}\mathbf{E} \end{aligned} \tag{88}$$

(Motion in (y, z) is neglected, the 3-D electromagnetic version of Equation (88) appears in Section 9).

The $\overline{\sum \cdot}$ term denotes for example a spatially averaged summed quantity and is included to enforce Galilean invariance. The solutions f_e and f_i of the Vlasov equations are functions of space variable x, velocity $\mathbf{v}$, and time. Ampere's equation is solved for the self-consistent electric field $\mathbf{E}$, which is a function of space variable x and time.

The boundary conditions used are periodicity in x, and zero at infinity in $|\mathbf{v}|$. Initial conditions which might be used for the distribution functions are from ref [15],

$$\begin{aligned} f_0(x, \mathbf{v}, \mathbf{u}_0, T_0) &= \frac{n_0(x)}{\sqrt{2\pi k_B T_0/m}}\exp\left(-\frac{m(\mathbf{v}-\mathbf{u}_0)^2}{2k_B T_0}\right) \\ n_0(x) = n(t=0, x) &= 1 + \alpha_n\cos(kx) \end{aligned} \tag{89}$$

where n_0, $\mathbf{u}_0$ and T_0 are the initial number density, initial fluid velocity and initial temperature respectively. The parameter α_n is the perturbation amplitude, k is its wave vector, and m is the species mass. It follows that the (scaled) momentum is given formally as

$$n\mathbf{u}_\alpha(x) = \int \mathbf{v} f_\alpha(x, \mathbf{v}, t)d\mathbf{v} \tag{90}$$

where f_α is the distribution function for species α at time t. (In practice the integral would be replaced by a sum over particles.)

Note that periodic boundary conditions are of limited value in practice, and attention should be given to minimal modifications of the above problem where there is

1. a flux of momentum across the domain (inflow and outflow boundary conditions)
2. reflection of particles at the boundaries
3. a source of plasma within the domain, and outflow boundaries
4. and where the spatial dimension corresponds to arc length s along a fieldline (implies n replaced by $n/|\mathbf{B}|$, cf. Section 5.1).

7 System 2-5: Spatially 1-D multispecies plasma model

7.1 Fluid model

For a multispecies plasma, there is a system of Boltzmann equations to be solved, one for each species, each of form in 3 spatial dimensions

$$\mathcal{L}_7 f_\alpha = \sum_\beta Q(f_\alpha, f_\beta) + s_\alpha \tag{91}$$

where $\mathcal{L}_7$ is the 7-D Lie derivative (space, velocity-space and time make up the $3+3+1=7$ dimensions, α, β are species labels and Q is the Boltzmann collision operator. The multispecies equations are derived following Grad [17, § 6] by substituting in Equation (91)

$$f_\alpha = \exp(-\lambda H_\alpha)\mathcal{F}_\alpha(x, \mathbf{v}, t) \tag{92}$$

where the flow of the Lie derivative is given by the Hamiltonian H_α and $\mathcal{F}_\alpha$ is a functional of moments of f_α, to include (dropping the suffix on f)

$$n = \int f d\mathbf{v}, \;\; \mathbf{u}_0 = \int f \mathbf{v} d\mathbf{v}, \;\; T = \int f v^2/2 d\mathbf{v} \tag{93}$$

The resulting system is linearised and solved by iteration to give the multispecies plasma fluid equations in Zhdanov [17, § 6]. There are believed to be typographical errors in Zhdanov, so cross-checking is needed.

To see Grad's approach applied to classical fluids see for example [18, § 8].

7.2 Coupling to particles

Other, less collisional species are to be treated as particles as in Section 6 and coupled via s_α. Mathematical forms for s_α will be guided by the emerging results from particles' method research.

8 System 2-6: Spatially 2-D plasma model incorporating velocity space effects

8.1 2-D interchange model with fluid neutrals

After P. Tamain (private communication), the equations for time advance of respectively electron number density n_e, "vorticity" ($\nabla \cdot \mathbf{E}^+$), electron energy $\mathcal{E}_e$, ion energy $\mathcal{E}_i$ and neutral number density n_n are respectively

$$\partial_t n_e + \nabla \cdot (n_e \mathbf{u}_e) = S_{n_e} - \frac{n_e}{\tau_{n_e}} \tag{94}$$

$$\partial_t \nabla \cdot \mathbf{E}^+ + \nabla \cdot \left(\nabla \cdot \left(\mathbf{u}_i \otimes \mathbf{E}^+\right)\right) = \nabla \cdot \left(n_i \left(\mathbf{u}_{\nabla Bi} + \mathbf{u}_{cx}\right) - \frac{1}{Z_i} n_e \mathbf{u}_{\nabla Be}\right) + \frac{1}{Z_i}\frac{n_e}{\tau_{n_e}} - \frac{n_i}{\tau_{n_i}} + \nabla \cdot \left(\nu \nabla_\perp \left(\nabla \cdot \mathbf{E}^+\right)\right) \tag{95}$$

$$\partial_t \mathcal{E}_e + \nabla \cdot (\mathcal{E}_e \mathbf{u}_e + p_e \mathbf{u}_e) = S_{\mathcal{E}_e} - \frac{\mathcal{E}_e}{\tau_{Ee}} + Q_{ie} + \nabla \cdot (\chi_{\perp e} n_e \nabla_\perp T_e) \tag{96}$$

$$\partial_t \mathcal{E}_i + \nabla \cdot (\mathcal{E}_i \mathbf{u}_i + p_i \mathbf{u}_i) = S_{\mathcal{E}_i} - \frac{\mathcal{E}_i}{\tau_{Ei}} - Q_{ie} + \nabla \cdot (\chi_{\perp i} n_i \nabla_\perp T_i) \tag{97}$$

$$\partial_t n_n = S_{n_n} + \nabla \cdot (D_n \nabla_\perp p_n) \tag{98}$$

where with the usual notation for species α pressure p_α, temperature T_α, charge state Z_i, species mass m_α, electric potential Φ and magnetic field $\mathbf{B}$,

ion number density $n_i = n_e$ (99)

$$\mathcal{E}_\alpha = \frac{3}{2} p_\alpha = \frac{3}{2} n_\alpha k_B T_\alpha, \quad \alpha = i, e \tag{100}$$

modified electric field $\mathbf{E}^+ = \frac{m_i}{Z_i e B^2}\left(n_i \nabla_\perp \Phi + \frac{1}{Z_i e} \nabla_\perp p_i\right)$ (101)

(102)

Perpendicular advection velocities:

$$\mathbf{u}_e = \mathbf{u}_{E\times B} + \mathbf{u}_{\nabla Be} + \mathbf{u}_{\text{diff}} \tag{103}$$

$$\mathbf{u}_i = \mathbf{u}_{E\times B} + \mathbf{u}_{\nabla Bi} + \mathbf{u}_{\text{diff}} + \mathbf{u}_{cx} \tag{104}$$

with

$$\mathbf{u}_{E\times B} = \frac{\mu_{cx}^2}{1+\mu_{cx}^2}\frac{\mathbf{B}\times\nabla\Phi}{B^2} \tag{105}$$

$$\mathbf{u}_{\nabla Bi} = \frac{\mu_{cx}^2}{1+\mu_{cx}^2}\frac{2T_i}{Z_i e B}\frac{\mathbf{B}\times\nabla B}{B^2} \tag{106}$$

$$\mathbf{u}_{\nabla Be} = -\frac{2T_e}{eB}\frac{\mathbf{B}\times\nabla B}{B^2} \tag{107}$$

$$\mathbf{u}_{cx} = \frac{\mu_{cx}}{1+\mu_{cx}^2}\frac{1}{B}\left(-\nabla_\perp \Phi - \frac{1}{Z_i e n_i}\nabla p_i\right) \tag{108}$$

$$\mathbf{u}_{\text{diff}} = -D_\perp \nabla n_e \tag{109}$$

with the magnetization with respect to charge exchange reactions defined as $\mu_{cx} = \frac{\omega_c}{\nu_{cx}}$, $\omega_c = \frac{Z_i e B}{m_i}$ being the ion cyclotron frequency and $\nu_{cx} = K_{cx} n_n$ the charge exchange frequency ($K_{cx}\left(n_i, T_i\right)$ the reaction rate of charge exchange reactions).

Loss rates can be given several meanings in this kind of model. They can be prescribed as parameters, but they can also describe sheath losses in which case they have a non-linear dependency with the plasma conditions, eg.

$$\tau_{n_e} = \frac{L_\parallel}{c_s} \exp\left(\Lambda_b - \frac{e\Phi}{T_e}\right) \tag{110}$$

$$\tau_{n_i} = \frac{L_\parallel}{c_s} \tag{111}$$

$$\tau_{\mathcal{E}_e} = \frac{2}{3\gamma_e} \tau_{n_e} \tag{112}$$

$$\tau_{\mathcal{E}_i} = \frac{2}{3\gamma_i} \tau_{n_i} \tag{113}$$

where $c_s = \sqrt{\frac{T_i + Z_i T_e}{m_i}}$ is the acoustic velocity and

$$\Lambda_b = -\frac{1}{2} \ln\left[0.5 \frac{m_e}{m_i}\left(1 + \frac{T_i}{T_e}\right)\right] \tag{114}$$

is the sheath potential drop normalized to T_e.

The collisional energy equipartition term (from Braginskii) is:

$$Q_{ie} = 3 \frac{m_e}{m_i} \frac{n_e}{\tau_{ce}} \left(T_e - T_i\right) \tag{115}$$

with the electron collision time given by:

$$\tau_{ce} = \frac{3\left(2\pi\right)^{3/2} \epsilon_0^2 \sqrt{m_e} T_e^{3/2}}{n_i {Z_i}^2 e^4 \Lambda} \tag{116}$$

and Λ is the Coulomb logarithm (which has a weak dependence on n_e and T_e as indicated in Section 2.2).

Source terms:

$$S_{n_e} = -S_{n_n} = n_e n_n K_i\left(n_e, T_e\right) - n_e^2 K_r\left(n_e, T_e\right) \tag{117}$$

$$S_{E_e} = -n_e n_n K_i\left(n_e, T_e\right) \mathcal{E}_i\left(T_e\right) - n_e^2 K_r\left(n_e, T_e\right) \frac{3}{2} T_e \tag{118}$$

$$S_{E_i} = -n_e^2 K_r\left(n_e, T_e\right) \frac{3}{2} T_i \tag{119}$$

where K_i and K_r are the ionization and recombination reaction rates.

Neutral diffusion coefficient:

$$D_n = \frac{1}{m_i\left(n_i K_{cx}(n_i, T_i) + n_e K_i(n_e, T_e)\right)} \tag{120}$$

Other perpendicular diffusion coefficients from Braginskii as in Section 2.2.

Boundary conditions:

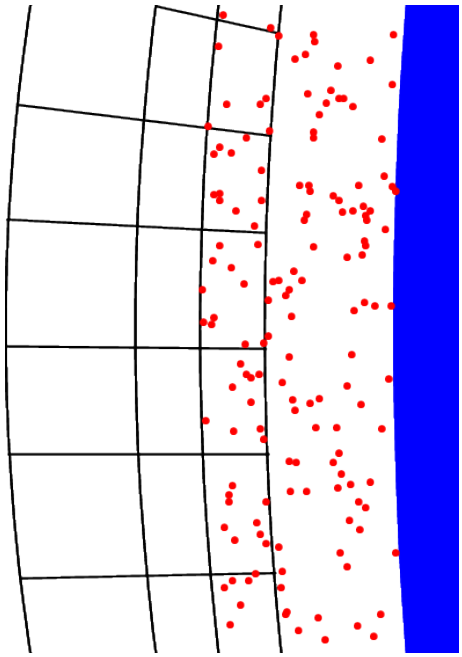

Figure 3: Handling a plasma sheath adjacent to wall at right. Plasma has fluid properties discretised using fe indicated using warped grid, but in sheath is better represented as particles indicated by dots.

- electron density n_e: zero flux
- electron energy E_e: zero flux
- ion energy E_i: zero flux
- electrostatic potential Φ: Dirichlet equal to average of $\Lambda_b T_e$ along the boundary
- neutral density n_n: incoming flux fixed by integral of particle losses in parallel direction (exact redistribution to be discussed)

8.2 Coupling to particles

The only appearance of particle or kinetic effects in the model of Section 8.1 is via the sheath boundary condition. A more detailed treatment of the sheath uses particle techniques cf. Section 7, where the different representation is used in a second overlapping region as indicated in Figure 3 taken from ref [19].

9 System 3-1: 2-D particle-based model of neutral gas and impurities with critical physics

The following generic transport equation [20, § 1] applies to

all particle-based models for the time evolution of the density distribution function $f(x, \mathbf{v}, t)$

$$\frac{\partial f}{\partial t} + \mathbf{v} \cdot \frac{\partial f}{\partial \mathbf{x}} + \mathbf{a} \cdot \frac{\partial f}{\partial \mathbf{v}} = S_C(f) = \left(\frac{\partial f}{\partial t} \right)_C + s_{exp}(\mathbf{x}, \mathbf{v}, t) \tag{121}$$

where $\mathbf{a} = d^2\mathbf{x}/dt^2$ is the acceleration experienced by a particle at position $\mathbf{x}$ with velocity $\mathbf{v}$. This represents scalar advection in a 6-D space with an explicit source $s_{exp}(\mathbf{x}, \mathbf{v}, t)$ and a source due to other inter-particle interactions that is conventionally written $(\partial f/\partial t)_C$ when it is localised and usually depends linearly on f.

Complete specification of the problem even for $S_C = 0$ and a single species of particle requires a force law such as that for particles of species α with charge q_α and mass m_α

$$\mathbf{F} = m_\alpha \frac{d^2\mathbf{x}}{dt^2} = q_\alpha(\mathbf{E} + \mathbf{v} \times \mathbf{B}) \tag{122}$$

and equations for the evolution of the electromagnetic fields $\mathbf{E}(\mathbf{x}, t)$ and $\mathbf{B}(\mathbf{x}, t)$ such as Maxwell's equations, neglecting displacement current. For neutral particles, when often $\mathbf{a} = \mathbf{0}$, interest attaches to S_C which for 2-particle interactions is often the Boltzmann operator for different species $Q(f_\alpha, f_\beta)$ where α, β are species labels.

It will be seen that Equation (121) is a statement that the $7 - D$ Lie derivative of f vanishes, and it is hoped that in the longer term, the properties of the Lie derivative might be exploited.

For current purposes, it is necessary to state a multi-species version of Equation (121) complete with appropriate source terms to represent the physics thought critical for modelling the tokamak edge. Inevitably choice of S_C is a function of lengthscale and timescale. On fast timescales in a strong electromagnetic field, the effect of collisions can be ignored (collective effects are felt through say the electrostatic field).

10 Summary

Acknowledgement

The support of the UK Meteorological Office and Strategic Priorities Fund is acknowledged. Valuable input from Ben Dudson is also acknowledged. Stuart Henderson provided helpful advice concerning plasma radiation.

References

[1] Proxy Applications. `https://proxyapps.exascaleproject.org`, 2020. Online; accessed May 2020.

[2] W. Arter, L. Anton, D. Samaddar, and R. Akers. ExCALIBUR Fusion Modelling System Science Plan. Technical Report CD/EXCALIBUR-FMS/0001, UKAEA, 2019. `https://www.metoffice.gov.uk/binaries/content/assets/metofficegovuk/pdf/research/spf/ukaea-excalibur-fms-scienceplan.pdf`.

[3] E.C. Howell and C.R. Sovinec. Solving the Grad–Shafranov equation with spectral elements. *Computer Physics Communications*, 185(5):1415–1421, 2014. `http://dx.doi.org/10.1016/j.cpc.2014.02.008`.

[4] J.P. Gunn, T. Hirai, Y. Corre, F. Escourbiac, A. Grosjean, and R.A. Pitts. A study of planar toroidal–poloidal beveling of monoblocks on the ITER divertor outer vertical target. *Nuclear Fusion*, 59(12):126043, 2019.

[5] R. Dejarnac, J.P. Gunn, P. Vondracek, M. Komm, R. Panek, and R.A. Pitts. Physics of toroidal gap heat loading on castellated plasma-facing components. *Nuclear Materials and Energy*, 19:19–27, 2019.

[6] J.D. Huba. NRL Plasma Formulary. Technical Report NRL/PU/6790–07-500, Naval Research Laboratory, Washington, 2007. Online version dated 2009 at `https://apps.dtic.mil/dtic/tr/fulltext/u2/a499299.pdf`.

[7] S.I. Braginskii. Transport Processes in a Plasma. In M.A.Leontovich, editor, *Reviews of Plasma Physics Vol.1*, pages 205–311. Consultants Bureau, New York, 1965.

[8] J.P. Goedbloed and S. Poedts. *Principles of magnetohydrodynamics: with applications to laboratory and astrophysical plasmas*. Cambridge University Press, 2004.

[9] J.A. Wesson. *Tokamaks, 3rd Edition*. Clarendon Press, Oxford, 2003.

[10] P.H. Roberts. *An Introduction to Magnetohydrodynamics*. Longmans, London, 1967.

[11] L.C. Appel, I. Lupelli, and JET Contributors. Equilibrium reconstruction in an iron core tokamak using a deterministic magnetisation model. *Computer Physics Communications*, 223:1–17, 2018.

[12] E. Havlíčková, W. Fundamenski, F. Subba, D. Coster, M. Wischmeier, and G. Fishpool. Benchmarking of a 1D scrape-off layer code SOLF1D with SOLPS and its use in modelling long-legged divertors. *Plasma Physics and Controlled Fusion*, 55(6):065004, 2013.

[13] D. Xiu and G. E. Karniadakis. Modeling uncertainty in flow simulations via generalized polynomial chaos. *Journal of computational physics*, 187(1):137–167, 2003.

[14] W. Arter, E. Threlfall, and J. Parker. Report on user layer design for Uncertainty Quantification. Technical Report CD/EXCALIBUR-FMS/0024-M3.1.3, UKAEA, 2020.

[15] W.T. Taitano, D.A. Knoll, L. Chacón, and G. Chen. Development of a Consistent and Stable Fully Implicit Moment Method for Vlasov–Ampère Particle in Cell (PIC) System. *SIAM Journal on Scientific Computing*, 35(5):S126–S149, 2013.

[16] G. Chen, L. Chacon, and D.C. Barnes. An energy-and charge-conserving, implicit, electrostatic particle-in-cell algorithm. *Journal of Computational Physics*, 230(18):7018–7036, 2011.

[17] V.M. Zhdanov. *Transport processes in multicomponent plasma*. CRC Press, 2002.

[18] W.B. Thompson. *An Introduction to Plasma Physics*. Pergamon, 1962.

[19] W. Arter, L. Anton, and D. Samaddar. Options for Particle Algorithms. Technical Report CD/EXCALIBUR-FMS/0013-1.01-M2.3.1, UKAEA, 2020.

[20] J.J. Duderstadt and W.R. Martin. *Transport Theory*. Wiley, 1979.

[21] L. Golub and J.M. Pasachoff. *The solar corona, 2nd Edition*. Cambridge University Press, 2010.

[22] V.A. Ambartsumyan, editor. *Theoretical Astrophysics, translated by J.B.Sykes*. Pergamon Press, 1958.

[23] M. O'Mullane. Atomic Processes in Plasmas. Slides from 45th Culham Plasma Physics Summer School, 2008. CCFE intranet, not publicly available.

[24] R.J. Bray and R.E. Loughhead. *Sunspots*. Dover Publications, 1964.

[25] The ADAS Project. Atomic Data and Analysis Structure ADAS website. `http://www.adas.ac.uk/`, 2020. Accessed: July 2020.

[26] The ADAS Project. Dissemination of atomic data and analysis structure adas website. `https://open.adas.ac.uk/`, 2020. Accessed: July 2020.

[27] Gwyn Williams. Electron Binding Energies. `https://userweb.jlab.org/~gwyn/ebindene.html`, 2000. Accessed: July 2020.

[28] H. Summers, M. O'Mullane, and A. Whiteford. ADAS: Atomic data, modelling and analysis for fusion. `https://icamdata2006.obspm.fr/documents/icam_pdf/Summers.pdf`, 2006. Slides from Meudon.

[29] N.R. Badnell, M.G. O'Mullane, H.P. Summers, Z. Altun, M.A. Bautista, J. Colgan, T.W. Gorczyca, D.M. Mitnik, M.S. Pindzola, and O. Zatsarinny. Dielectronic recombination data for dynamic finite-density plasmas-I. Goals and methodology. *Astronomy & Astrophysics*, 406(3):1151–1165, 2003.

[30] J.-Ch. Sublet, J.W. Eastwood, J.G. Morgan, M.R. Gilbert, M. Fleming, and W. Arter. FISPACT-II: An Advanced Simulation System for Activation, Transmutation and Material Modelling. *Nuclear Data Sheets*, 139:77–137, 2017. `http://dx.doi.org/10.1016/j.nds.2017.01.002`, website: `https://fispact.ukaea.uk/`.

[31] S.S. Henderson, M. Bluteau, A. Foster, A. Giunta, M.G. OMullane, T. Pütterich, and H.P. Summers. Optimisation and assessment of theoretical impurity line power coefficients relevant to ITER and DEMO. *Plasma Physics and Controlled Fusion*, 59(5):055010, 2017.

[32] S.S. Henderson, M.M. Bluteau, M.G. OMullane, and H.P. Summers. Improvements of impurity line ITER and DEMO via systematic optimisation of atomic structure. Technical Report UKAEA-CCFE-PR(18)31, CCFE, 2018.

A Annex A: Atomic and Molecular Effects

Often the radiation emitted and absorbed by atoms in different ionisation states must be accounted for. There is a compact introduction in Golub and Pasachoff [21, § 3.3.1]. This explains how in principle, given a "particular mixture of elements at a specified temperature . . . the number of atoms per unit volume of the gas which are in a particular ionisation state may be calculated . . . then for that atom which emission lines are emitted" and so on for all other constituents of the mixture. (Temperature refers to a black-body radiation field in which the atoms are assumed to sit.) "The sum total of all these bound-bound emissions, plus the bound-free and free-free emissions" is the spectrum, where it is explained that 'bound' and 'free' describe the state of the electron involved in the formation of the line with respect to the atom. But "in practice, carrying out this calculation is . . . enormously complicated".

The complication follows from the range of competing mechanisms even within atoms of one element, namely the bound-bound mechanisms of decay and excitation described in ref [21, § 3.2.1], and bound-free of recombination and photo-emission, because of the different possible degrees of ionisation as atomic number A increases and because the proportion of atoms in each ionisation state depends on the proportions in the others.

Ambartsumyan [22, § 5] explains at greater length the calculation in *thermal equilibrium* of the proportion of different ions for each element [22, § 5.2], then the bound-free / free-bound coefficients (§ 5.3—§ 5.5) and free-free (§ 5.6). In [22, § 24.1–24.2] there is a discussion of metastable states, which in the astrophysical context are crucial for the formation of forbidden lines in nebulae, but may also be important in the context of fusion because these metastable atomic states can survive for many seconds at low densities of matter and of radiation. By metastable state is meant that no transition to it from lower energy levels of the electrons is possible except for the so-called 'forbidden', less probable electric quadrupole interactions from the quantum-mechanical matrix elements.

The above outlines the main physics issues. From O'Mullane's slides at the 2008 Summer School [23], the main difference between astrophysics and fusion application seems to be that in the plasma context, if it is used, Saha's ionisation formula needs modification by the Saha-Boltzmann deviation factors b_n or 'b-factors' ref [23, slide 21]. The Zeeman effect is also neglected, although this might be expected to be important, as from its use in sunspot observation [24, § 5.2] spectral line splitting by wavelengths of 0.1 nm is expected.

The key observation is from O'Mullane [23] that in tokamak modelling, there are two distinct uses for atomic data - (1) to calculate source (loss) terms for species time evolution equations, and (2) to compute synthetic spectra, ie. intensity as a function of frequency. The latter (2) is by far the more involved but it is only critical for diagnosticians working with particular apparatus. Indeed, Golub and Pasachoff [21, § 3.3.2] go on to argue that for an optically thin plasma, the radiation (in W/m^3) could be expressible as simply as

$$E_R = n_e n_p P(T) \tag{123}$$

where n_p accounts for the number density of the plasma ions and $P(T)$ is the emitted power integrated over all wavelengths for a plasma with a specified mix of elements. The separate functions used to compute $P(T)$ depend mainly on electron temperature with a weak dependence on density. The form of $P(T)$ as a result of the integration over spectrum always seems to be smooth. It would seem to be a prime candidate for precomputation as a function of the fractions of the major plasma species, and could be approximated very efficiently because of the smoothness.

O'Mullane [23] give a more detailed result, namely that there is a source/sink term for electron energy of form

$$S_e = -E_R = n_e \sum_s \sum_{Z=0}^{Z=Z_0(s)} P^Z n^Z - I^Z \left(\mathcal{S}^{Z \to Z_p} n^Z + \alpha^{Z_p \to Z} n^{Z_p} \right) \tag{124}$$

where Z is charge state, the suffix s on the density has been dropped, $Z_m = Z - 1$, $Z_p = Z + 1$, and where $Z_0(s)$ is the number of charge states of species s included in the model. It may be inferred that

$$\mathcal{S}^{Z_m \to Z} \text{ or } \mathcal{S}^{Z \to Z_p} = \text{ionisation coefficient} \tag{125}$$

$$\alpha^{Z \to Z_m} \text{ or } \alpha^{Z_p \to Z} = \text{partial dielectronic recombination rate coefficient} \tag{126}$$

$$P^Z = \text{radiated power per atom of } n^Z \tag{127}$$

$$I^Z = \text{power per atom released in dielectronic recombination} \tag{128}$$

where the coefficients, as elsewhere in this section, are expected to be obtained from the Atomic Data and Analysis Structure ADAS database [25, 26]. The data requirements for this look relatively modest, assuming the coefficients for each species and charge state are smooth functions of temperature only. Thus if say $N_T \approx 20$ samples specify these functions and $Z_{sum} = \sum_s Z_0(s)$, then the total number of coefficients required could be estimated as $Z_{sum} \times 3 \times N_T \approx 20 \times 3 \times 10 = 600$ where if the number of different elements present $N_s = 10$, and if the average number of charge states $\bar{N}_Z = 2$, then $Z_{sum} = N_s \bar{N}_Z \approx 20$. In another case of interest, a calculation might include only two or three extra species if one were Tungsten (W), so $N_s = 4$ but then $N_Z = 22$ for W alone if $T_e > 40$ eV [27].

The number densities n^Z for each charge state may be straightforwardly calculated by solving a transport equation for each isotope n_s and using the Saha-Boltzmann formula modified with b-factors to determine the distribution of charge states. (Further, for heavier elements a mean atomic mass may be used to avoid separate treatment of isotopic species.) Much more serious implications for computation [23], arise in the time evolution equations if each charge state is treated separately. This may be necessary in a strong electric field because each different ion feels a different electromagnetic force. An ion of species s with charge state Z will acquire a source

$$S_s^Z = \mathcal{S}^{Z_m \to Z} n_e n^{Z_m} - \left(\alpha^{Z \to Z_m} + \mathcal{S}^{Z \to Z_p}\right) n_e n^Z + \alpha^{Z_p \to Z} n_e n^{Z_p} \tag{129}$$

where again the suffix s on the density has been dropped. Thus the demands on atomic data are not very different from those for the energy equation, but since the total cost of these additional computations with $Z_0(s)$ extra species will scale at least as fast as $Z_{sum} = \sum_s Z_0(s)$ (inter-species coupling may add considerably to the computational expense), rendering negligible the cost of inputting a few thousand coefficients from disc. In practice a useful surrogate is produced by replacing separate ionisation states by 'superstages' (slide 17 of ref [28]), where one superstage corresponds to one electron shell of the atom. However, even the smaller number of 7 superstages required for W might double or treble the length of a typical computation.

The above is typically as much detail as is sensible to consider under heading (1). If detailed diagnostics under (2) are required, the generalised collisional-radiative (GCR) model [29] gives an idea of the computational demands. GCR modelling requires each metastable state to be considered separately, since each has a separate finite lifetime. It helps that the transport of each atom in the state is presumably the same, but even so there is a need to solve a rate equation for metastable state density at sample points throughout the computational domain The source terms are complicated, namely for the metastable state labelled ρ

$$\begin{aligned}
S_\rho^Z / n_e &= \sum_\sigma \mathcal{X}_{\sigma\to\rho}^{Z\to Z} n_\sigma - \sum_\sigma \mathcal{X}_{\rho\to\sigma}^{Z\to Z} n_\rho && (130)\\
&+ \sum_\mu \mathcal{S}_{\mu\to\rho}^{Z_m\to Z} n_\mu^{Z_m} - \sum_\nu \mathcal{S}_{\rho\to\nu}^{Z\to Z_p} n_\rho && (131)\\
&+ \sum_\nu \alpha_{\nu\to\rho}^{Z_p\to Z} n_\nu^{Z_p} - \sum_\mu \alpha_{\rho\to\mu}^{Z\to Z_m} n_\rho && (132)\\
&+ \sum_\sigma \mathcal{Q}_{\sigma\to\rho}^{Z\to Z} n_\sigma - \sum_\sigma \mathcal{Q}_{\rho\to\sigma}^{Z\to Z} n_\rho && (133)
\end{aligned}$$

where the superfix Z as well as the suffix s on the density has been dropped and the new symbols are

$$\begin{aligned}
\mathcal{X}_{\sigma\to\rho}^{Z\to Z} &= \text{generalised collisional-radiative (GCR) excitation coefficient} && (134)\\
\mathcal{Q}_{\sigma\to\rho}^{Z\to Z} &= \text{parent-metastable cross-coupling coefficient} && (135)
\end{aligned}$$

Note that the expressions in both ref [29, eq. (9)] and ref [23, slide 41] appear to contain typos, and that the meanings of $\mathcal{X}$ and $\mathcal{Q}$ have swapped. Each of the new terms contains approximately $8M_Z$ coefficients where M_Z is the number of metastable states for species s (which includes the ground state). It may be inferred from refs [23, 28] that the number of metastable states for a given ionisation Z is relatively small (slide 9 of ref [28] indicates that all ionisation states for Oxygen

have $M_z \leq 4$; slide 19 suggests $M_Z \leq 6$ for W when $Te < 100\,\text{eV}$). The coefficients $\mathcal{X}, \mathcal{S}, \mathcal{Q}$ in Equation (130) are functions of electron density as well as temperature so may require at least 100 sample points to specify, hence the total data can be estimated as $Z_{sum} \times M_Z \times 8 M_Z \times 100$. However FISPACT-II [30] experience with rate equations indicates the cost of these additional computations with M_Z metastables far exceeds the cost of inputting of order ten or so thousand coefficients from disc.

Where the demands of data might become important is in the translation of the n_σ^Z into spectral lines. First the regular excited states, because they equilibrate on the usual atomic timescales which are negligible compared to plasma timescales, are calculated using a purely algebraic relation [29, eq. (5)],

$$n_i^Z / n_e = \sum_\sigma {}^X\mathcal{F}_{i\sigma} n_\sigma^Z + \sum_\mu {}^I\mathcal{F}_{i\mu} n_\mu^{Z_m} + \sum_\nu {}^R\mathcal{F}_{i\nu} n_\nu^{Z_p} \tag{136}$$

where ${}^{X,I,R}\mathcal{F}_{i\sigma}$ are the coefficients of excitation, ionisation and recombination for the transition from metastable state σ to regular excited state i, each is a function of n_e and T_e with corresponding storage requirement of order 100. Equation (136) requires $Z_{sum} \times M_S \times M_Z$ $\mathcal{F}$ coefficients where M_S is the number of states, which is potentially infinite, and indeed in practice could be as large as ≈ 500, necessitating the use of 'bundling' of the higher energy states to reduce the number to manageable proportions, say 10 [29]. Next, as explained in the opening paragraph, to each state there corresponds a description of its spectrum, which may contain many separate lines, each described by its wavelength, relative amplitude and a profile shape which may require several further parameters to describe. Mitigating the demand for coefficient data, is the fact that the diagnostics need only be computed intermittently.

To treat atomic physics UQ in a later stage of NEPTUNE, a Monte-Carlo calculation might be considered, involving all the different interactions between all the metastable states where the Maxwellian assumption is relaxed, posing a multiscale multiphysics problem. However, the validity of this approach requires further consideration as Henderson et al [31] also indicates that even as recently as 2017, errors of 30 % were present in important coefficients, although the discrepancies have now been reduced to approximately 5 % [32].